ROYAL SOCIETY
OF CHEMISTRY

PAPER

Check for updates

Selective adsorption and determination of doxorubicin and epirubicin in plasma using magnetic molecularly imprinted polymers combined with HPLC-UV

Shukai Sun,[a] Yue Zhai,[a] Qingwu Tian,[a] Peng Zhao,[a] Hong Cheng,[b] Deng Pan, [ID] [a] Junna Sui,[a] Yusun Zhou,[a] Chao Xuan*[a] and Tingting Zhou [ID] *[a]

Magnetic molecularly imprinted polymers (MMIPs) were synthesized using magnetic $Fe_3O_4@SiO_2$ as a carrier for the selective recognition and adsorption of doxorubicin (DOX) and epirubicin (EPI) in plasma. Then, the method was combined with high-performance liquid chromatography-ultraviolet detection (HPLC-UV) to realize rapid and accurate detection of DOX and EPI concentrations in plasma. The structures of the prepared MMIPs were characterized by X-ray diffraction, transmission electron microscopy, X-ray photoelectron spectroscopy, and magnetic saturation. As observed, the prepared MMIPs had a uniform appearance and excellent magnetic properties. Then, the adsorption performance of MMIPs was verified through static, dynamic, and selective adsorption tests. MMIPs were found to have high adsorption capacity (8.36 and 8.19 mg g^{-1}), high selectivity (imprinting factors of 34.83 and 8.03), and rapid adsorption for DOX and EPI, respectively. Next, HPLC-UV was used for quantitative analysis. The prepared method had a good linear relationship (0.0001–0.5 mg mL^{-1} for DOX and 0.0002–0.5 mg mL^{-1} for EPI) and low detection limits (0.04613 ng mL^{-1} for DOX and 0.08969 ng mL^{-1} for EPI). The combination of magnetic solid-phase extraction and HPLC-UV was a highly specific and sensitive method for determining DOX and EPI concentrations in plasma.

1. Introduction

Doxorubicin (DOX), an anthracycline compound originally isolated from *Streptomyces peucetius*, has broad-spectrum antitumor activity against multiple cancer types including breast cancer, lymphoma, leukemia, brain cancer, and lung cancer.[1,2] Epirubicin (EPI) is a differential isomer of DOX, which inhibits DNA and RNA synthesis by intercalating between base pairs; it is also an anthracycline with broad-spectrum antitumor activity.[3] However, given that such drugs have a short half-life, high hydrophilicity, large distribution, and low bioavailability, their therapeutic effect is only evident at high doses.[4] In addition, when the blood concentration reaches a certain limit, these drugs lack tumor specificity and can induce myocardial cytotoxicity,[5] renal function injury,[6] testicular cytotoxicity,[7] and bone marrow hematopoietic inhibition.[8] The concentration of drugs in a patient's body plays an important decisive role in cell biological events that lead to cell arrest or death.[9] Therefore,

monitoring the levels of these drugs in a patient's body during treatment is crucial.

To date, various analytical techniques have been used to detect DOX and EPI, including electrochemical methods,[10] capillary electrophoresis,[11] high-performance liquid chromatography (HPLC),[12] and fluorescence.[13] However, the application of these approaches in clinical is limited due their poor selectivity, complex operation, long measurement time, and costly instruments and equipment.[14–16] Therefore, a method for detecting drug concentration with high stability, low cost, simple and rapid operation, and reliable results needs to be developed.

Molecularly imprinted polymers (MIPs) are three-dimensional polymers comprising template molecules, functional monomers, and crosslinkers.[17] After removing template molecules, MIPs contain tailored cavities which are complementary to the template molecules in both size and functional groups. This type of pore has a specific recognition effect on the template molecules and their structural analogs, and it can be specifically adsorbed to the imprinted pore when the template molecules appear again.[18] As a result, MIPs exhibit high selectivity and specificity for target molecule adsorption, demonstrating a specific recognition capability comparable to that of biological antibodies. MIPs have low preparation cost, fast

[a]*Department of Clinical Laboratory, The Affiliated Hospital of Qingdao University, No. 1677, Wutaishan Road, Qingdao 266000, Shandong, China. E-mail: zhouting81205@163.com; cxuan@mail.nankai.edu.cn*

[b]*Department of Medical, The Affiliated Hospital of Qingdao University, Qingdao 266000, Shandong, China*

preparation speed, good stability, and excellent reproducibility; they have been widely used and are further developed in the biological field at present.[19] At present, there are studies on the use of MIPs of doxorubicin for drug sustained release,[20] but there is currently no research on their application in chromatographic detection. There is no research related to MIPs of epirubicin.

In recent years, magnetic MIPs (MMIPs) have been developed by combining molecular imprinting with magnetic separation technologies, creating novel materials capable of efficiently isolating target molecules and specifically recognizing.[21] MMIP is a new type of material comprising Fe_2O_3 or Fe_3O_4 magnetic particles and a non-magnetic polymer matrix. Using an external magnetic field instead of centrifugation or filtration in the separation step greatly simplifies the extraction process. In addition, magnetic materials are easy to functionalize for improving their selectivity, which makes them a simple, environmentally friendly, and efficient adsorbent for sample pretreatment methods. These materials have been widely used in different fields such as chemistry, biology, and medicine.[22]

Biological samples contain a large number of macromolecular compounds, which cause intense interference to the detection of target objects. Moreover, the content of target objects in biological samples is usually very low, which requires the use of sample pretreatment technology to extract biological samples for removing the interference substances.

Magnetic solid-phase extraction (MSPE) uses MMIP as an extraction material to separate and enrich organic and inorganic analytes from samples. It has large specific surface area, multiple binding sites, strong adsorption performance, good selectivity, and easy separation. Notably, it reduces the loss during solid separation, which further improves the enrichment coefficient, and enhances the sensitivity of detection.[23] Pengli Jian *et al.*[24] applied micro-solid-phase extraction method with molecularly imprinted membrane protection to detect the content of local anesthetics in cosmetics. The detection range of local anesthetics can reach 0.01–0.71 mg L^{-1}, which confirmed that the MIP has good imprinting property and selectivity, and the micro-solid-phase extraction device is simple, low cost, and reusable. The combination of HPLC and ultraviolet detection (HPLC-UV) is an effective method for drug analysis due to its high separation efficiency.[25] This research team has jointly applied MSPE and HPLC-UV technology to establish a detection method for methotrexate (MTX). The linear range is within 0.00005–0.25 mg mL^{-1}, and the detection limit can reach 12.51 ng mL^{-1}. The accuracy of MTX detection by the MSPE/HPLC-UV method is high. The results were consistent with those of a drug concentration analyzer.[26]

The present study aimed to establish a rapid, accurate, and sensitive assay for detecting DOX and EPI in plasma. To this end, novel MMIPs were synthesized for the extraction and enrichment of DOX and EPI samples from plasma samples. The adsorption properties of MMIPs and the MSPE process were systematically studied. A method of material preparation, sample processing, and sample determination was established by combining the MSPE technique with HPLC.

2. Materials and methods

2.1. Reagents

Pure methanol, ethanol, acetonitrile, ammonium hydroxide, potassium hydroxide, $FeCl_3 \cdot 6H_2O$, and $FeSO_4 \cdot 7H_2O$ were derived from Sinophosphine Chemical Reagent Co., Ltd (Shanghai). 3-Aminopropyl triethoxysilane (APTES, 98%) and tetraethyl orthosilicate (TEOS, 98%) were obtained from Sigma-Aldrich (St. Louis, MO, USA); Doxorubicin hydrochloride (98%), roxithromycin (98%), azithromycin, dixithromycin, and clarithromycin were supplied by Shanghai Macklin Biochemical Company. Erythromycin was provided by Shanghai Tixiai Chemical Industrial Development Company. Acetic acid was obtained from Yantai Far East Fine Chemical Co., Ltd. Di-erythromycin (97%) were purchased from Shanghai Aladdin Biochemical Technology Co., Ltd. Epirubicin hydrochloride was purchased from Hebei Bailingwei Hyperfine Materials Co., Ltd.

2.2. Instruments

The precision electronic balance was purchased from Sartorius (Goettingen, Germany). The thermostatic water bath box was provided by Tuan electromechanical Automotive Equipment Co., Ltd (Changsha, China). The air drying box was purchased from Shanghai Yiheng Scientific Instrument Co., Ltd (Shanghai, China). The oscillator was supplied by Scilogex (Pittsburgh, PA, USA). The KQ-50DB type CNC ultrasonic cleaner was provided by China Kunshan Ultrasonic Instrument Co., Ltd (Jiangsu, China). The electric mixer was purchased from Meiyingpu Instrument Manufacturing Co., Ltd (Shanghai, China). The Merinton SMA4000 ultramicrospectrophotometer (Beijing, China) was utilized. Shimadzu LC-20AT HPLC chromatograph was purchased from Shimadzu Corporation (Japan, Jingdong), and the chromatograph column (C18) was obtained from Waters (Milford, MA, USA). The X-ray photoelectron spectrometer (XPS) was provided by Thermo Fisher Scientific (Waltham, MA, USA). The transmission electron microscope (JEM 1200EX) was provided by Electron Optics Laboratory (Tokyo, Japan). The X-ray diffractometer was provided by Panalytical (Almelo, Netherlands). The vibrating sample magnetometer (VSM) was supplied by MicroSense Corporation (USA).

2.3. Synthesis of Fe_3O_4 NPs

Fe_3O_4 NPs was synthesized according to our previous work,[27] the process was addressed below simply. 0.6 g of $FeCl_3 \cdot 6H_2O$ and 0.35 g of $FeSO_4 \cdot 7H_2O$ were dissolved in deionized water (10 mL) for neutralization. Then, they were filtered using a 0.22 μm water-based filter membrane. Under the protection of nitrogen, a three-nozzle flask containing of deionized water (120 mL) was heated in a water bath to 80 °C. Next, the filtrate was added to the three-nozzle flask and stirred with a whisk at 260 rpm for 30 min. Thereafter, ammonia water (5 mL) was added, and continue stirred for 30 min. Once completed, the material was cooled to room temperature and washed with deionized water and ethanol for three times. The mass of Fe_3O_4 synthesized in a single batch was approximately 200 ± 10 mg, while multiple syntheses yielded around 400 mg. 10 mL of deionized water was

added to Fe_3O_4 (400 mg), which obtained a colloidal solution of 40 mg mL^{-1} for further use.

2.4. Synthesis of $Fe_3O_4@SiO_2$

The synthesis of $Fe_3O_4@SiO_2$ was according to our previous work[27] with little modification, the detail were below. 80 mL of methanol and 20 mL of deionized water were added to the three-neck bottle. 10 mL colloidal solution of Fe_3O_4 NPs at 400 mg mL^{-1} and 1 mL of ammonia solution were introduced, and ultrasonic dispersion was conducted for 5 min. The flask was equipped with a mechanical mixer and stirred at 450 rpm for 10 minutes in a 30 °C water bath 2.5 mmol of TEOSwas dissolved in anhydrous ethanol (1 mL) to create a silicon mixed solution. The silicon mixture was added to the three-neck bottle, and stirring was continued for 6 h. $Fe_3O_4@SiO_2$ was separated using an external magnetic field, and then washed twice with ethanol and deionized water. Then the prepared $Fe_3O_4@SiO_2$ was added to deionized water (40 mL) to produce a colloidal solution of $Fe_3O_4@SiO_2$ for later use, with which concentration was 12.25 mg mL^{-1}.

2.5. Preparation of MMIPs and MNIPs

In this study, MMIPs were prepared *via* the sol–gel method using doxorubicin hydrochloride as template. 80 mL of methanol solution was poured into a three-neck flask, then 0.6 mmol of doxorubicin hydrochloride and 300 μL of ammonia were added. Ultrasonic mixing was then performed. The three-neck flask was fixed on a mechanical agitator and mechanically stirred at 260 rpm at room temperature for 10 min. A 20 mL colloidal solution of $Fe_3O_4@SiO_2$ at 12.25 mg mL^{-1} was added, and stirring was continued for 6 min. After 15 min, 1 mL of ammonia was added, followed by 1.2 mmol of APTES. After an additional 30 min, 3.6 mmol of TEOS was introduced, and the reaction was allowed to continued for 16 h.

The polymer obtained in the three-neck flask was MMIPs. The MMIPs were washed three times with a methanol solution, followed by washing with a 0.1 M potassium hydroxide solution and a methanol mixture (1 : 1,v/v) to remove the template molecules in the synthetic MMIPs until the supernatant was no longer colored and no doxorubicin hydrochloride was detected by HPLC-HV. Finally, the polymers underwent three successive washings with methanol. Following this, the product was dried at 45 °C for 12 h. Magnetic non-imprinted polymers (MNIPs) were prepared samely, but doxorubicin hydrochloride was not added in the synthesis process.

2.6. Adsorption experiments and characterization of MMIPs and MNIPs

DOX and EPI solutions of different concentrations were prepared with methanol and distilled water (1 : 1,v/v), and MMIPs and MNIPs of appropriate amounts were added and mixed using an oscillator. The absorbance of DOX and EPI in the supernatant was detected using an ultra-microspectrophotometer at regular intervals, and the concentration of the supernatant was calculated according to the standard curve. Also, dynamic, static and selective adsorption

experiments were conducted using this method. Three polymers ($Fe_3O_4@SiO_2$, MMIPs, and MNIPs) were characterized by transmission electron microscopy (TEM), X-ray diffractometer (XRD), X-ray photoelectron spectroscopy (XPS), and vibrating sample magnetometry (VSM).

2.7. MSPE process

A total of 200 μL of normal plasma without DOX and EPI was added to 40 mL of methanol, followed by ultrasound mixing. The heart was then subjected to separation at 8000 rpm for 5 min, and the supernatant was the collected as the serum treatment solution. MMIPs (100 mg) were placed into a 15 mL centrifuge tube. Then, 10 mL of methanol was introduced and oscillated for 5 min. After the activation was completed, the supernatant was discarded through magnetic separation. A total of 400 μL of a 0.25 mg mL^{-1} standard solution of DOX and EPI, as well as 4.6 mL of plasma treatment solution, was added to a centrifuge tube containing 100 mg of MMIPs. The final concentration of DOX and EPI was 0.02 mg mL^{-1}. The sample was vibrated at room temperature for 240 min to complete extraction and loading, followed by magnetic separation and post-MMIPS recovery. Following sample loading, 5 mL of a water–methanol (9 : 1, v/v) leaching solution was added and the mixture was then vortexed for 1 minute. The residual impurities were removed by washing, followed by recovery of the material. Finally, add 5 mL of acetic acid eluent to the recovered MMIPs and oscillate the mixture for 60 minutes. After magnetic separation, transfer the collected material to a test tube. Dry it under a stream of nitrogen and then dissolve it in 500 μL of a methanol–water mixture (1 : 1, v/v). HPLC-UV detection was performed after filtered through 0.22 μm organic filter membrane.

2.8. HPLC-UV analysis

HPLC-UV (SHIMADZU) was employed to detect DOX and EPI. The filtered 500 μL solution was placed in a liquid injection bottle and placed in the sample box. The chromatographic column in this study was C18 (5 μm, 150 mm × 4.6 mm). The optimized parameters were: the sample size was 20 μL, the flow rate was 0.5 mL min^{-1}, the detection wavelength was 254 nm, the mobile phase consisted of 30% acetonitrile and 70% PBS buffer (pH 2.8), and the column temperature was 30 °C.

2.9. Sample preparation and ethical statement

A total of 200 μL of normal plasma without DOX and EPI was added into 40 mL of methanol, followed by ultrasound mixing. Then, the heart was separated at 8000 rpm for 5 min, and the supernatant was treated as the plasma. Three 15 mL centrifuge tubes were prepared, with each containing 100 mg of MMIPs and 4.5 mL of the abovementioned plasma treatment solution. Thereafter, 500 μL of DOX and EPI solutions at 0.5, 0.2, and 0.1 mg mL^{-1} was added and mixed at room temperature for 6 h. The leaching and elution steps followed the same procedure as the MSPE method. The samples were tested by HPLC-UV.

All experiments were performed in accordance with the Guidelines of Helsinki Declaration (1996 edition), and

experiments were approved by the ethics committee at the Medical Ethics Committee of the Affiliated Hospital of Qingdao University. Informed consents were obtained from human participants of this study.

3. Results and discussion

3.1. Preparation of MMIPs

Now, aomounts of inorganic nanoparticles have been employed as the core materials for the synthesis of MIPs, silicon dioxide (SiO_2),[28] ferric oxide (Fe_3O_4),[29] silver (Ag),[30] and quantum dots (QDs),[31] for example. Fe_3O_4 particles has large specific surface area, good modifiability, excellent magnetic properties for rapid separation. In this work, Fe_3O_4 was selected as the core material. Fe_3O_4 was first synthesized *via* the co-precipitation method.[32] Then, $Fe_3O_4 @SiO_2$ of core–shell structure was synthesized with silicon coating to improve its antioxidant ability. MMIPs and MNIPs were prepared with APTES as the monomer and TEOS as the crosslinking agent.[33]

The ratio and amount of template, monomer, and cross-linker have effects on adsorption capacity of the polymers towards DOX and EPI. Thus, this study explored the optimized ratios of the template, monomer, and crosslinker. The experimental results are shown in Tables 1 and 2. Adsorption capacity refers to the amount of DOX and EPI (Q_{MMIPs} and Q_{MNIPs}) adsorbed by MMIPs and MNIPs. Notably, a larger value corresponds to a stronger adsorption capacity. Recognition ability is expressed as imprinting factor (IF = Q_{MMIPs}/Q_{MNIPs}), and a higher value indicates a stronger recognition specificity.

Tables 1 and 2 show that, 1 : 2 : 6 is the optimal ratio for template, monomer, and crosslinker, for the adsorption capacity of the MMIPs for DOX and EPI is larger at 8.36 mg g^{-1} and 8.19 mg g^{-1}, while the imprinting factor (IF = Q_{MMIPs}/Q_{MNIPs}) is the largest at 34.83 and 8.02. These values are

significantly higher than those for other ratios, which suggests that the MIP has the strongest recognition ability for DOX and EPI. Considering the factors of Q_{DOX}, Q_{EPI}, and IF, the ratio of template, monomer, and crosslinker was selected as 1 : 2 : 6.

3.2. Relevant adsorption experiments

A study was conducted to optimize the experimental conditions for the static and dynamic adsorption properties of the polymer, aiming to evaluate the adsorption capacity of MMIPs towards DOX and EPI. 20 mg of MMIPs powder and 20 mg of MNIP powders were placed in a 1.5 mL EP tube after weighed. Methanol–aqueous solutions (1 : 1, v/v) were prepared with 0.5 mg mL^{-1} of DOX and EPI solutions and diluted into 0.25, 0.1, 0.05, 0.02, and 0.01 mg mL^{-1} concentration gradients. A total of 0.05–0.01 mg mL^{-1} of DOX and EPI solutions were added into EP tubes containing 20 mg of MMIP powder and 20 mg of MNIP powder, respectively. Then, they were mixed for 12 h. For magnetic separation, the adsorption amounts of DOX and EPI by MMIPs and MNIPs were calculated by measuring the concentrations of DOX and EPI in the supernatant. Then, static adsorption curves were drawn. The corresponding results are shown in Fig. 1A.

The adsorption capacity of MMIPs for DOX and EPI increases significantly with the rise in DOX and EP concentrations. At the same concentration of DOX and EPI, the binding amount of MMIPs is significantly higher than that of MNIPs. This result is due to the formation of molecularly imprinted holes corresponding to the target material on the surface of the MMIP. This phenomenon increases the specific adsorption of MMIPs to DOX and EPI. The dynamic adsorption curve provides insight into the adsorption kinetics and allows for the determination of the equilibrium time. Subsequently, 100 mg portions of both MMIPs and MNIPs powders were accurately weighed and transferred into separate 15 mL centrifuge tubes. A total of

Table 1 The influence of the composition of template, monomer, and crosslinker on the adsorption perfprmance of MMIPs for DOX

Template: monomer: crosslinker	Q_{DOX} (mg g^{-1}) (MMIPs)	Q_{DOX} (mg g^{-1}) (MNIPs)	IF (Q_{MMIPs}/Q_{MNIPs})
1 : 1 : 6	5.94	0.42	14.14
1 : 2 : 6	8.36	0.24	34.83
1 : 3 : 6	8.73	1.12	7.79
1 : 4 : 6	9.00	2.34	3.84
1 : 5 : 6	9.30	6.19	1.50
1 : 6 : 6	5.94	6.64	0.92

Table 2 The influence of the composition of template, monomer, and crosslinker on the adsorption perfprmance of MMIPs for EPI

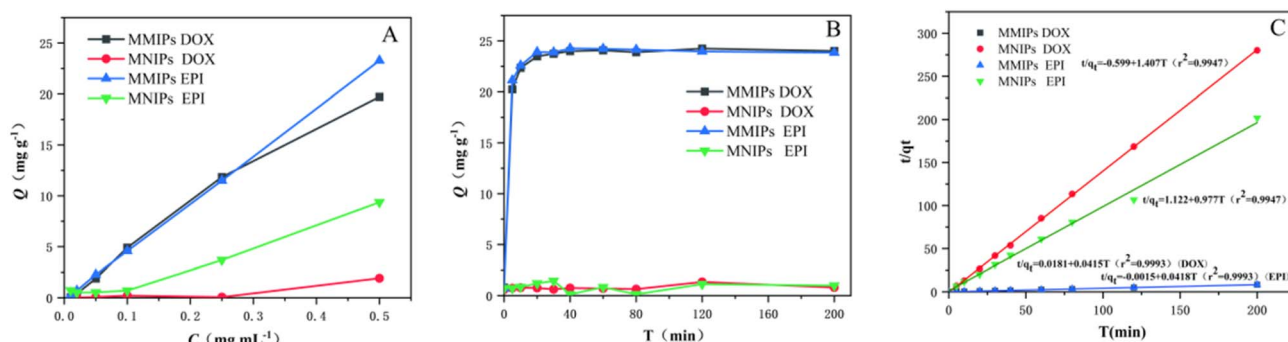| Template: monomer: crosslinker	Q_{EPI} (mg g^{-1}) (MMIPs)	Q_{EPI} (mg g^{-1}) (MNIPs)	IF (Q_{MMIPs}/Q_{MNIPs})
1 : 1 : 6	6.27	0.89	7.04
1 : 2 : 6	8.19	1.02	8.02
1 : 3 : 6	8.52	1.68	5.07
1 : 4 : 6	8.97	3.16	2.84
1 : 5 : 6	9.18	7.64	1.20
1 : 6 : 6	5.70	6.39	0.89

Fig. 1 Static adsorption curves (A), dynamic adsorption curves (B) and dynamic adsorption kinetic fitting curves (C).

10 mL of a DOX and EPI methanol–aqueous solution (1 : 1, v/v) at 0.25 mg mL^{-1} was added into the 15 mL centrifuge tube, followed by shaking and mixing at room temperature. After magnetic separation at 0, 5, 10, 20, 30, 40, 60, 80, 120, and 200 min, 1 mL of the supernatant was withdrawn, and the concentration of DOX and EPI in the supernatant was determined. The dynamic changes in the adsorption capacity of DOX and EPI by MMIPs and MNIPs were observed, as shown in Fig. 1B.

The adsorption curve of MMIPs increases rapidly as time progresses. It reaches equilibrium at 30 min, which indicates that these polymers have high adsorption rate and excellent adsorption capacity. Conversely, the adsorption curve of MNIPs rises slowly, and the increasing trend is not obvious at any time, which suggests their slower adsorption rate and weaker adsorption capacity. The results reveal that the imprinting pores on the surface of MMIPs can quickly and selectively adsorb DOX and EPI, and the adsorption capacity is very strong.

To analyze the kinetic data of MMIPs and MNIPs, a pseudo-second-order model was applied. The corresponding equations and fitting results are presented below:

$$\frac{t}{q_t} = \frac{1}{k_2 \times q_e{}^2} + \frac{t}{q_e} = \frac{1}{v_0} + \frac{1}{q_e} \tag{1}$$

where q_t denotes the adsorption capacity (mg g^{-1}) at time t, and qe represents the adsorption capacity (mg g^{-1}) at equilibrium. k_2 stands for the rate constant of the pseudo-second-order model (g mg^{-1} min^{-1}). v_0 indicates the initial adsorption rate. As illustrated in Fig. 1C, a plot of t/q_t ratio and t exhibits a strong linear relationship, with a correlation coefficient (r^2) exceeding 0.99. These results demonstrate that the pseudo-second-order model provides a satisfactory fit for describing the dynamic adsorption processes of DOX and EPI on both MMIPs and MNIPs.

3.3 Selective evaluation

Seven aliquots each containing 20 mg of MMIP powder and seven aliquots each containing 20 mg of MNIP powder were separately weighed and transferred into 1.5 mL EP tubes. A methanol–aqueous (1 : 1, v/v) solution containing 0.25 mg mL^{-1} of DOX, EPI, and their structural analogs-including di-rithromycin, roxithromycin, erythromycin, azithromycin, and

clarithromycin-was serially diluted to generate concentration gradients of 0.1, 0.05, 0.02, and 0.01 mg mL^{-1}. The adsorption of DOX, EPI, and their structural analogs on MMIPs and MNIPs is shown in Fig. 2. MMIPs have the highest adsorption capacity for DOX and EPI, but the adsorption capacity for DOX and EPI analogs is very low. The adsorption effect of MMIPs on DOX and EPI is better than that of MMIPs on structural analogs. The reason is that the pores on MMIPs can only specifically accommodate DOX and EPI. This finding further indicates that MMIPs have a good selective recognition ability for DOX and EPI. However, it should be pointed out that for its metabolites doxorubicinol and epirubicinol, due to their extremely similar structures, selective adsorption may not be achieved well. Therefore, in the presence of metabolites, it is necessary to enhance material selectivity groups or chromatographic separation capabilities to separate them from metabolites.

3.4 Characterization of MMIPs and MNIPs

The TEM images in Fig. 3 depict the three polymers (Fe$_3$O$_4$@-SiO$_2$, MMIPs, and MNIPs). Fig. 3A illustrates Fe$_3$O$_4$@SiO$_2$ particles with a discernible polymer layer on their surface, which indicates successful silicon coating of the Fe$_3$O$_4$ NPs.

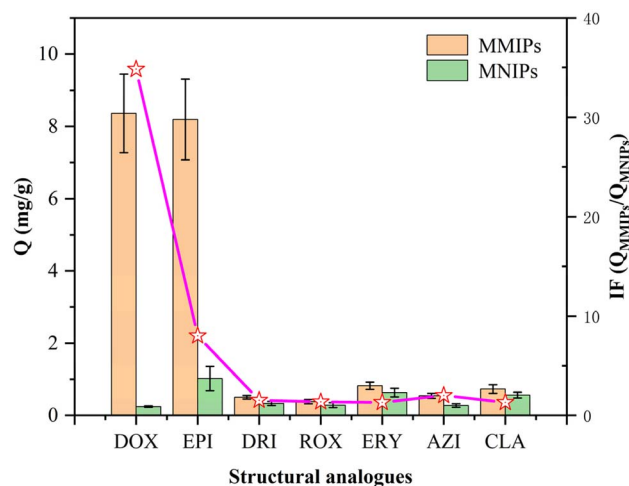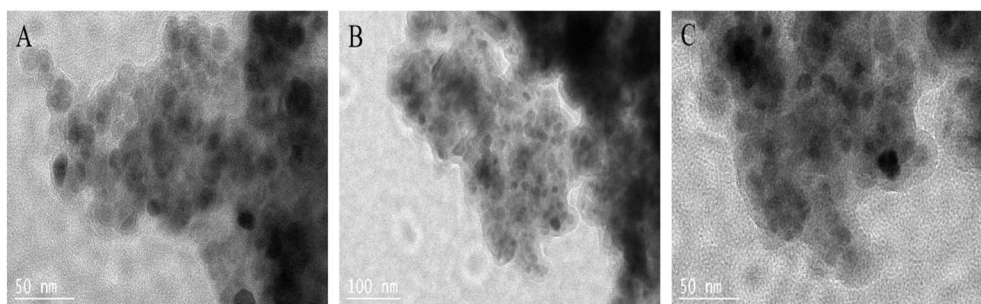**Fig. 2** Adsorption properties of MMIPs and MNIPs on DOX, EPI, and their structural analogs.

Fig. 3 TEM images of three polymers (A) (Fe_3O_4@SiO_2), (B) (MMIPs), and (C) (MNIPs).

Fig. 3B and C present the electron microscopy images of MMIPs and MNIPs, respectively. The formation of a polymer layer on the surface of Fe_3O_4@SiO_2 provides clear evidence of the successful synthesis of both MMIPs and MNIPs. Notably, MMIPs possess a slightly larger diameter than MNIPs due to the wider imprinting chamber present in MMIPs.

The XRD spectra of a polymer can reflect its crystal structure. As shown in Fig. 4, the six crystal face constants of Fe_3O_4@SiO_2 correspond to the characteristic peaks occurring at $2\theta = 30.10°$, $35.51°$, $43.15°$, $53.59°$, $56.95°$, $62.70°$, which are consistent with related reports.[34] In addition, MMIPs and MNIPs show the same peaks, which implies that the crystal structure of Fe_3O_4 does not change during the preparation process.

Fig. 5 exhibt the XPS spectra of the polymers. The Fe 2p peak observed at 710.98 eV indicates the presence of Fe_3O_4 in all three polymers (Fig. 5B). The O 1s peaks at 530.2 eV can be attributed to Fe–O, C=O, C–O, and Si–OvSi bonds (Fig. 5C). The peak binding energy of si 2p is 103.17 eV, which reflects the presence of Si–O–Si (Fig. 5D). Therefore, Fe_3O_4 NPs is successfully coated with silica. Moreover, the peak binding energy of 401.84 eV exists in $-NH_2$ (Fig. 5A), which implies the successful synthesis of MMIPs and MNIPs.

Ms can evaluate the magnetic strength of magnetic substances. Fig. 6 shows the hysteresis curves of Fe_3O_4@SiO_2, MMIPs, and MNIPs. As shown in the figure, Fe_3O_4@SiO_2 has an

Ms of 69.5 emu g^{-1}, MMIPs have an Ms of 60.5 emu g^{-1}, and MNIPs have an Ms of 30.5 emu g^{-1}. Therefore, Fe_3O_4@SiO_2 has the strongest magnetic properties, and the magnetic properties of MMIPs decrease after the composite material is synthesized. MNIPs have the lowest magnetic properties, but the magnetic properties of MMIPs and MNIPs can still meet the requirements of rapid magnetic separation.

3.5 Optimization of MSPE conditions for enriching DOX and EPI

3.5.1. Optimization of sample loading conditions. Loading is the first step of solid-phase extraction, and the selection of loading conditions has a significant impact on the solid-phase extraction process. Therefore, we optimized the conditions that affect loading. As shown in Fig. 7A, when the amount of MMIPs and MNIPs was 100 mg, the recovery of DOX and EPI were highest, therefore, the optimized amount for MMIPs and MNIPs in MSPE process was 100 mg. Another influencing factor is the loading time, as shown in Fig. 7B. When the loading time is 240 minutes, the extraction recovery rate reaches stability. Therefore, in subsequent experiments, the loading time is chosen to be 240 minutes.

3.5.2. Choice of leaching solution. The eluent washes away the interfering substances on the surface of MMIPs while minimizing the loss of DOX and EPI that have been adsorbed in MMIPs. In this experiment, the leaching solution was composed of water and methanol. At the end of the leaching process, the concentrations of DOX or EPI in the leaching supernatant were measured. The effect of different volume ratios of the leaching solutions on MSPE performance was evaluated. As illustrated in Fig. 8, when the water-to-methanol volume ratio is 9 : 1, the difference in chromatographic peak area between MMIPs and MNIPs leachates reaches a minimum, indicating an optimal leaching efficiency. As a result, water–methanol (9 : 1, v/v) was selected as the leaching agent.

3.5.3. Selection of elution parameters. The optimal eluant must be selected to achieve the highest extraction recovery. The influence of different proportions of methanol–acetic acid solution on extraction recovery was observed using methanol–acetic acid solution as the eluent. The influence of the ratio of methanol to acetic acid in the eluent on the extraction recovery of DOX and EPI is shown in Fig. 9. As the proportion of acetic acid increases gradually, the recovery rate rises gradually. When
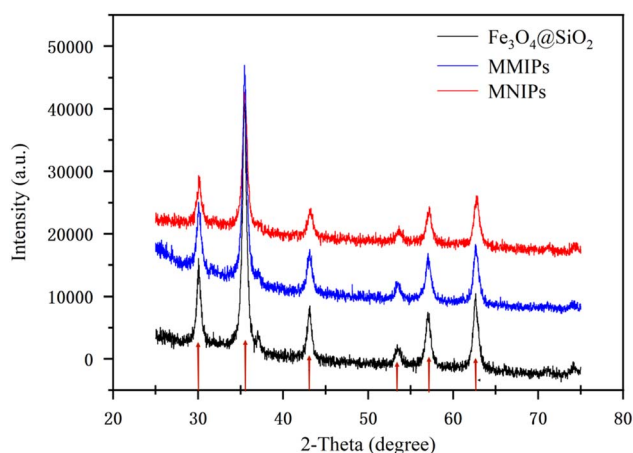

Fig. 4 XRD patterns of three polymers (Fe_3O_4@SiO_2, MMIPs, and MNIPs).

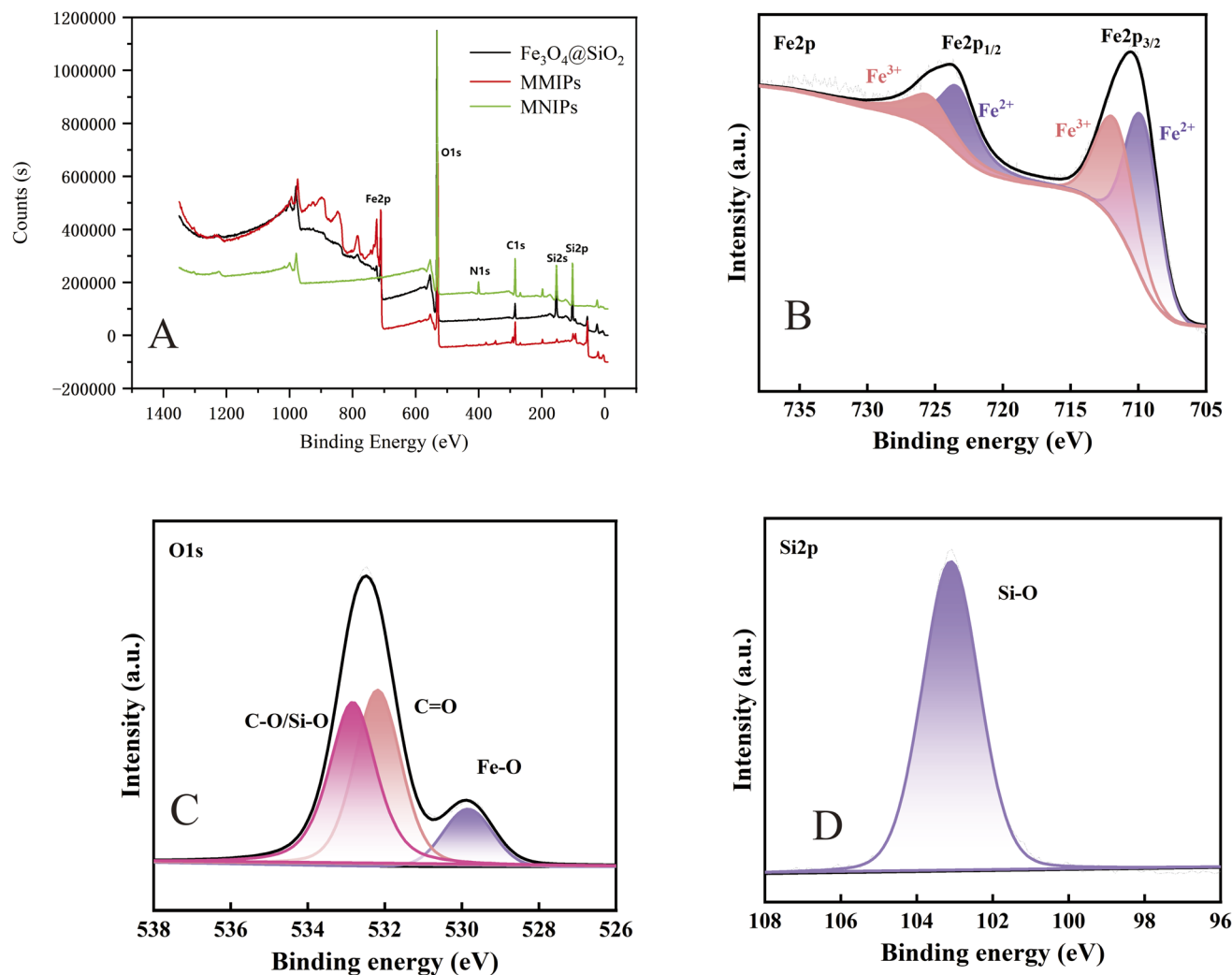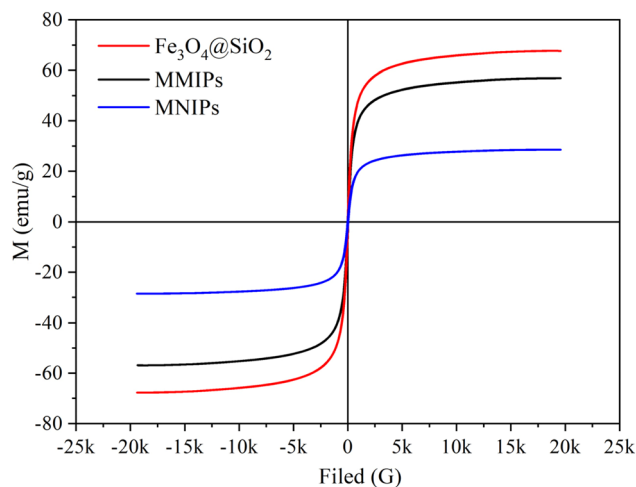**Fig. 5** XPS spectras (A–D) of three polymers ($Fe_3O_4@SiO_2$, MMIPs, and MNIPs).

Fig. 6 VSM analysis for three polymers ($Fe_3O_4@SiO_2$, MMIPs, and MNIPs).

the eluent is pure acetic acid, the extraction recovery rate is the highest. The values are 101.57 and 94.87, which imply that acetic acid can effectively elude DOX and EPI molecules from the cavity of MMIPs. Accordingly, acetic acid was used as the ideal eluent in subsequent experiments.

3.5.4. Method verification. First, a standard curve method using MSPE/HPLC-UV was established for detecting DOX and EPI in spiked solutions, as shown in Fig. 10. The results indicate that DOX exhibits a linear response within the concentration range of 0.0001–0.5 mg mL^{-1}, with a linear regression equation of $Y = 5E + 07X + 70\,923$ ($R^2 = 0.9999$). Similarly, EPI measured using the standard addition method shows a linear relationship in the range of 0.0002–0.5 mg mL^{-1}, following the equation $Y = 5E + 07X + 55\,130$ ($R^2 = 0.9998$). According to the signal-to-noise ratio (S/N = 3), the detection limit of DOX is 0.04613 ng mL^{-1}, and that of EPI is 0.08969 ng mL^{-1}. The LODs achieved by this method are lower than the typical spiked concentrations of DOX and EPI, demonstrating its suitability for monitoring blood concentrations of both compounds. It can also expand the detection range of DOX and EPI.
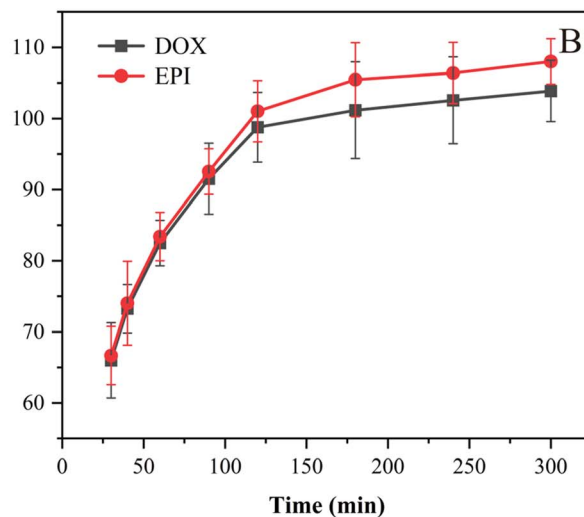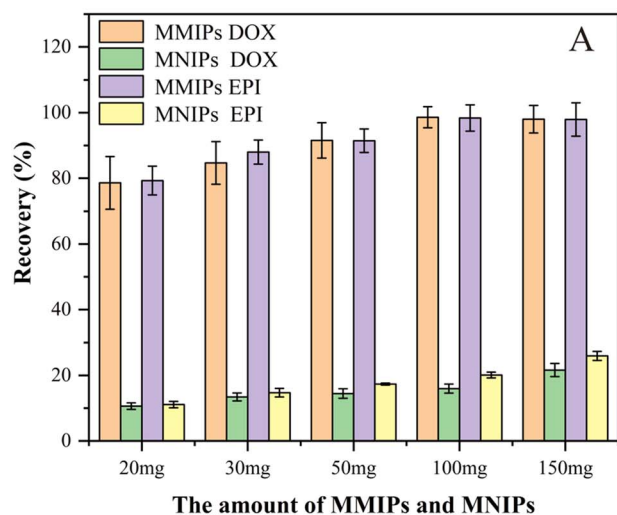
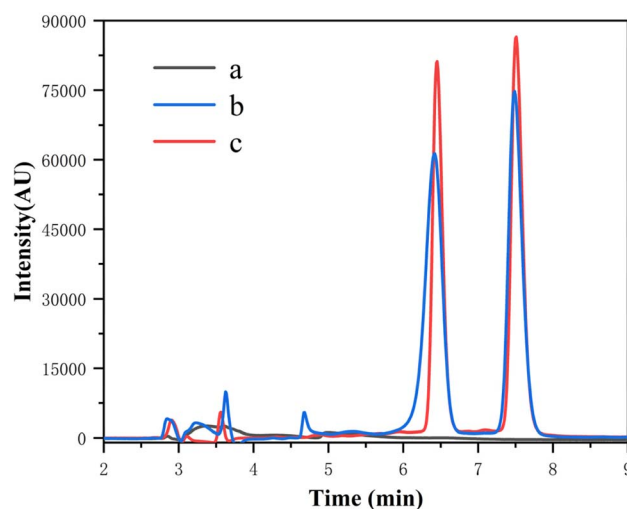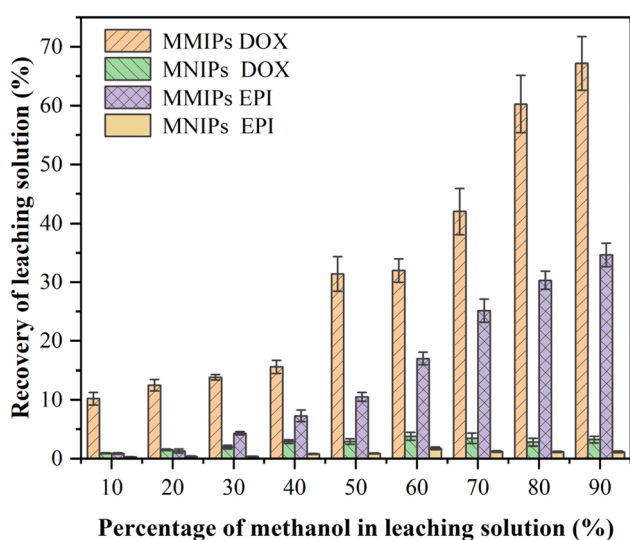Fig. 7 Optimization of the amount of MMIPs and MNIPs.

Fig. 8 Optimization of elution parameters of MMIPs and MNIPs.

Fig. 9 Optimization of percentage of acetic acid in the extraction solution in the MSPE process.

Fig. 10 HPLC of the three solutions: blank baseline (a), DOX and EPI standard solution (b, 0.05 mg mL^{-1}), and spiked solution extracted by MMIPs (c, 0.05 mg mL^{-1}).

To evaluate the performance of the developed MSPE/HPLC-UV method, a comparative analysis was conducted between this approach and other reported methods for the determination of DOX and EPI, as summarized in Tables 3 and 4. The results demonstrate that the present method exhibits satisfactory superiority in terms of sensitivity, detection limit, or other key metrics.

3.6. Measurement of DOX and EPI in serum

The plasma treatment solution was prepared by treating human plasma with methanol. A 500 μL solution containing DOX and EPI at 0.5, 0.2, and 0.1 mg mL^{-1} was added. Then, the plasma specimens were treated by the MSPE method. As shown in Tables 5 and 6, the average recovery rate ($n = 3$) was used to evaluate the accuracy of DOX and EPI concentrations at different concentration levels of 0.05, 0.02 and 0.01 mg mL^{-1}, respectively. The relative standard deviation (RSD) value was

used to estimate the precision. In general, the recovery rates of DOX range from 85.62% to 112.22%, and the RSD value is less than 6%. The recoveries of EPI range from 89.51% to 116.56%, and the RSD value is less than 6%. The concentrations of DOX and EPI in the samples were analyzed using HPLC-UV, with the results presented in Fig. 10. The findings indicate that the MSPE/HPLC-UV method effectively resists interference from plasma matrix components and successfully enriches both DOX and EPI. Moreover, the detection methods developed in this study exhibit high efficiency, delivering accurate and practical outcomes. They are also applicable for the determination of these analytes in actual plasma samples.

Table 3 Comparison of DOX detection between this work and other reported works

Recognition element	Linearity range	Method LODs	References
Aptamer-based biosensor		28 nM	35
Electrochemical	98.3–1218 μM	31 nM	10
Fluorescence bioprobe	25–100 mg	25 ng mL^{-1}	36
HPLC		4.5 fmol mL^{-1}	37
Liquid chromatography with fluorescence	1–1000 ng mL^{-1}	0.5 ng mL^{-1}	38
MSPE/HPLC-UV	0.0001–0.5 mg mL^{-1}	0.04613 ng mL	This work

Table 4 Comparison of EPI detection between this study and other reported works

Recognition element	Linearity range	Method LODs	References
Quantum dots		0.04×10^{-6} mol L^{-1}	39
Aptasensor based on structure-switching aptamer	0.07–1.0 μM and 1.0–21.0 μM	0.04 μM	40
Electrochemical	0.01–500 μM	6.3 nM	41
Deep eutectic solvent	0.001–500 μM	0.8 nM	42
Reverse-phase HPLC with UV detection	0.016–1.024 μg mL^{-1}	0.016 μg mL^{-1}	43
MSPE/HPLC-UV	0.0002–0.5 mg mL^{-1}	0.08969 ng mL^{-1}	This work

Table 5 Experiment for the recovery of DOX additive

Samples	Added (mg mL^{-1})	Found (mg mL^{-1})	Recovery (%)	Average recovery (%)	RSD (%)
1	0.01	0.008249	82.49		
	0.01	0.008771	87.71	85.62	2.76
	0.01	0.008666	86.66		
2	0.02	0.02231	111.54		
	0.02	0.02149	107.44	112.22	5.15
	0.02	0.02354	117.68		
3	0.05	0.04914	98.28		
	0.05	0.04787	95.74	97.29	1.36
	0.05	0.04892	97.84		

Table 6 Experiment for the recovery of EPI additive

Samples	Added (mg mL^{-1})	Found (mg mL^{-1})	Recovery (%)	Average recovery (%)	RSD (%)
1	0.01	0.008702	87.02	96.08	1.64
	0.01	0.009076	90.76		
	0.01	0.009076	90.76		
2	0.02	0.02403	120.15		
	0.02	0.02348	117.39	115.56	5.72
	0.02	0.02183	109.14		
3	0.05	0.04723	94.46		
	0.05	0.04803	96.05	89.51	2.16
	0.05	0.04887	97.74		

4. Conclusion

In this study, a combined MSPE/HPLC-UV method was developed utilizing molecularly imprinted magnetic polymers (MMIPs) as the solid-phase extraction adsorbent, enabling efficient adsorption and selective recognition of doxorubicin (DOX) and epirubicin (EPI) in plasma samples. Several characterizations, including TEM, XRD, XPS, and VSM, verified the successful synthesis of the composite and its good magnetic response. The synthesized MMIPs exhibit high adsorption capacity, rapid sorption kinetics, strong selectivity, and excellent practical applicability. HPLC-UV exhibits good specificity and high sensitivity. This study demonstrates that the combination of MSPE with HPLC-UV provides a novel and straightforward approach for determining the concentrations of DOX and EPI in plasma. This understanding provides methodological support for the clinical detection of DOX and EPI concentrations.

Conflicts of interest

The authors assert that no personal connections or competing financial interests exist that could have had an impact on the work presented in this paper.

Data availability

Data for this article are available at https://github.com/gisnew/ztt/blob/main/Datas.xlsx.

Acknowledgements

References

1 S. Y. van der Zanden, X. Qiao and J. Neefjes, New insights into the activities and toxicities of the old anticancer drug doxorubicin, *FEBS J.*, 2021, **288**(21), 6095–6111.

2 A. M. Mohamed, H. R. Al-Qalawi, W. A. El-Sayed, W. A. Arafa, M. S. Alhumaimess and A. K. Hassan, Anticancer activity of newly synthesized triazolopyrimidine derivatives and their nucleoside analogs, *Acta Pol. Pharm.*, 2015, **72**(2), 307–318.

3 K. Nagai, S. Fukuno, M. Shiota, M. Tamura, S. Yabumoto and H. Konishi, Differences in Transport Characteristics and Cytotoxicity of Epirubicin and Doxorubicin in HepG2 and A549 Cells, *Anticancer Res.*, 2021, **41**(12), 6105–6112.

4 B. S. Chhikara, D. Mandal and K. Parang, Synthesis, anticancer activities, and cellular uptake studies of lipophilic derivatives of doxorubicin succinate, *J. Med. Chem.*, 2012, **55**(4), 1500–1510.

5 S. Salinger-Martinovic, V. Cosic, N. Stojiljkovic, S. Ilic, N. Stojanovic and T. Dencic, Impact of ellagic acid application on doxorubicin-induced cardiovascular toxicity model, *Can. J. Physiol. Pharmacol.*, 2021, **99**(2), 185–191.

6 H. Qi, J. Fu, J. Luan, C. Jiao, X. Cui, X. Cao, *et al.*, miR-150 inhibitor ameliorates adriamycin-induced focal segmental glomerulosclerosis, *Biochem. Biophys. Res. Commun.*, 2020, **522**(3), 618–625.

7 K. K. Karna, B. R. Choi, J. H. You, Y. S. Shin, K. K. Soni, W. S. Cui, *et al.*, Cross-talk between ER stress and mitochondrial pathway mediated adriamycin-induced testicular toxicity and DA-9401 modulate adriamycin-induced apoptosis in Sprague-Dawley rats, *Cancer Cell Int.*, 2019, **19**, 85–96.

8 C. M. Fan, Y. W. Su, P. R. Howe and C. J. Xian, Long Chain Omega-3 Polyunsaturated Fatty Acid Supplementation Protects Against Adriamycin and Cyclophosphamide Chemotherapy-Induced Bone Marrow Damage in Female Rats, *Int. J. Mol. Sci.*, 2018, **19**(2), 484–499.

9 A. M. Meredith and C. R. Dass, Increasing role of the cancer chemotherapeutic doxorubicin in cellular metabolism, *J. Pharm. Pharmacol.*, 2016, **68**(6), 729–741.

10 S. V. Selvi, A. Prasannan, S. M. Chen, A. Vadivelmurugan, H. C. Tsai and J. Y. Lai, Glutathione and cystamine functionalized MoS(2)core-shell nanoparticles for enhanced electrochemical detection of doxorubicin, *Mikrochim. Acta*, 2021, **188**(2), 35–47.

11 S. M. Ansar, W. Jiang and T. Mudalige, Direct quantification of unencapsulated doxorubicin in liposomal doxorubicin formulations using capillary electrophoresis, *Int. J. Pharm.*, 2018, **549**(1–2), 109–114.

12 C. Siebel, C. Lanvers-Kaminsky, G. Würthwein, G. Hempel and J. Boos, Bioanalysis of doxorubicin aglycone metabolites in human plasma samples-implications for doxorubicin drug monitoring, *Sci. Rep.*, 2020, **10**(1), 18562–18569.

13 L. Zorić, N. Drinković, V. Micek, L. Frkanec, A. E. Türeli, N. Günday-Türeli, *et al.*, High-Throughput Method for the Simultaneous Determination of Doxorubicin Metabolites in Rat Urine after Treatment with Different Drug Nanoformulations, *Molecules*, 2022, **27**(4), 1177–1190.

14 W. G. Choi, D. K. Kim, Y. Shin, R. Park, Y. Y. Cho, J. Y. Lee, *et al.*, Liquid Chromatography-Tandem Mass Spectrometry for the Simultaneous Determination of Doxorubicin and its Metabolites Doxorubicinol, Doxorubicinone, Doxorubicinolone, and 7-Deoxydoxorubicinone in Mouse Plasma, *Molecules*, 2020, **25**(5), 1254–1267.

15 S. Jahandari, M. A. Taher, H. Karimi-Maleh and G. Mansouri, Simultaneous voltammetric determination of glutathione, doxorubicin and tyrosine based on the electrocatalytic effect of a nickel(II) complex and of Pt:Co nanoparticles as a conductive mediator, *Mikrochim. Acta*, 2019, **186**(8), 493–500.

16 P. Giraudeau, Challenges and perspectives in quantitative NMR, *Magn. Reson. Chem.*, 2017, **55**(1), 61–69.

17 L. Chen, X. Wang, W. Lu, X. Wu and J. Li, Molecular imprinting: perspectives and applications, *Chem. Soc. Rev.*, 2016, **45**(8), 2137–2211.

18 D. S. Villarreal-Lucio, K. X. Vargas-Berrones, L. Díaz de León-Martínez and R. Flores-Ramíez, Molecularly imprinted polymers for environmental adsorption applications, *Environ. Sci. Pollut. Res. Int.*, 2022, **29**(60), 89923–89942.

19 Z. El-Schich, Y. Zhang, M. Feith, S. Beyer, L. Sternbæk, L. Ohlsson, *et al.*, Molecularly imprinted polymers in biological applications, *BioTechniques*, 2020, **69**(6), 406–419.

20 M. Ceglowski, J. Kurczewska, P. Ruszkowski, J. Liberska and G. Schroeder, The influence of cross-linking agent onto adsorption properties, release behavior and cytotoxicity of doxorubicin-imprinted microparticles, *Colloids Surf., B*, 2019, **182**, 110379–110386.

21 J. Li, Y. Wang and X. Yu, Magnetic Molecularly Imprinted Polymers: Synthesis and Applications in the Selective Extraction of Antibiotics, *Front. Chem.*, 2021, **9**, 706311–706327.

22 S. Ansari and M. Karimi, Recent configurations and progressive uses of magnetic molecularly imprinted polymers for drug analysis, *Talanta*, 2017, **167**, 470–485.

23 S. Jia, Y. Zhou, J. Li, B. Gong, S. Ma and J. Ou, Highly selective enrichment and direct determination of imazethapyr residues from milk using magnetic solid-phase extraction based on restricted-access molecularly imprinted polymers, *Anal. Methods*, 2021, **13**(3), 426–435.

24 P. Jian, T. Muhammad, A. Wei, B. Wu and T. Zhou, A membrane-protected micro-solid-phase extraction method based on molecular imprinting and its application to the determination of local anesthetics in cosmetics, *J. Separ. Sci.*, 2022, **45**(14), 2675–2686.

25 D. Z. Yang, X. X. Yin, C. N. Ong and D. Q. Tang, Multidimensional information-based HPLC technologies to evaluate traditional chinese medicine, *J. Chromatogr. Sci.*, 2013, **51**(7), 716–725.

26 T. Zhou, Z. Deng, Q. Wang, H. Li, S. Li, X. Xu, *et al.*, Magnetic Molecularly Imprinted Polymers for the Rapid and Selective Extraction and Detection of Methotrexatein Serum by HPLC-UV Analysis, *Molecules*, 2022, **27**(18), 6084–6098.

27 T. Zhou, Z. Deng, Q. Wang, H. Li, S. Li, X. Xu, *et al.*, Magnetic molecularly imprinted polymers for the rapid and selective extraction and detection of methotrexatein serum by HPLC-UV analysis, *Molecules*, 2022, **27**(18), 6084–6098.

28 T. Kubo, S. Yamamoto, Y. Watabe, T. Tanigawa, D. Nakajima and K. Otsuka, Selective Separation of Thyroid-Hormone-Receptor-Binding Substances Using Molecularly Imprinted Polymers, *ACS Appl. Bio Mater.*, 2022, **5**(11), 5210–5217.

29 Y. Li, X. Zhang and J. Liu, Preparing Selective Nanozymes by Molecular Imprinting, *Methods Mol. Biol.*, 2021, **2359**, 223–232.

30 H. Wang, L. Cai, W. Hao, Y. Wang, G. Fang and S. Wang, Melamine-Ag with dual functions of electrochemiluminescence luminophore and coreactant accelerators: Construction of MIP/M-Ag@MoS(2)-QDs sensing platform for specific detection of thiabendazole, *Food Chem.*, 2023, **425**, 136472–136479.

31 P. Sawetwong, S. Chairam, P. Jarujamrus and M. Amatatongchai, Enhanced selectivity and sensitivity for colorimetric determination of glyphosate using Mn-ZnS quantum dot embedded molecularly imprinted polymers combined with a 3D-microfluidic paper-based analytical device, *Talanta*, 2021, **225**, 122077–122086.

32 A. E. Albalawi, A. K. Khalaf, M. S. Alyousif, A. D. Alanazi, P. Baharvand, M. Shakibaie, *et al.*, Fe3O4(@)piroctone olamine magnetic nanoparticles: Synthesize and therapeutic potential in cutaneous leishmaniasis, *Biomed. Pharmacother.*, 2021, **139**, 111566–111573.

33 Q. Cai, Z. Yang, N. Chen, X. Zhou and J. Hong, Selective capture and rapid identification of Panax notoginseng metabolites in rat faeces by the integration of magnetic molecularly imprinted polymers and high-performance liquid chromatography coupled with orbitrap mass spectrometry, *J. Chromatogr. A*, 2016, **1455**, 65–73.

34 L. Fu, Q. Chen, J. Chen, L. Ren, L. Tang and W. Shan, Magnetic carbon nanotubes-molecularly imprinted polymer coupled with HPLC for selective enrichment and determination of ferulic acid in traditional Chinese medicine and biological samples, *J. Chromatogr., B: Anal. Technol. Biomed. Life Sci.*, 2021, **1180**, 122870–122878.

35 N. Bahner, P. Reich, D. Frense, M. Menger, K. Schieke and D. Beckmann, An aptamer-based biosensor for detection of doxorubicin by electrochemical impedance spectroscopy, *Anal. Bioanal. Chem.*, 2018, **410**(5), 1453–1462.

36 Y. Liu and B. Danielsson, Rapid high throughput assay for fluorimetric detection of doxorubicin-application of nucleic acid-dye bioprobe, *Anal. Chim. Acta*, 2007, **587**(1), 47–51.

37 S. Ahmed, N. Kishikawa, K. Ohyama, M. Wada, K. Nakashima and N. Kuroda, Selective determination of doxorubicin and doxorubicinol in rat plasma by HPLC with photosensitization reaction followed by chemiluminescence detection, *Talanta*, 2009, **78**(1), 94–100.

38 O. Maliszewska, A. Plenis, I. Olędzka, P. Kowalski, N. Miękus, E. Bień, *et al.*, Optimization of LC method for the quantification of doxorubicin in plasma and urine samples in view of pharmacokinetic, biomedical and drug monitoring therapy studies, *J. Pharmaceut. Biomed. Anal.*, 2018, **158**, 376–385.

39 G. R. Bardajee, M. Sharifi and H. Mahmoodian, Novel CMC-CdTe/ZnS QDs Nanosensor for the Detection of Anticancer Drug Epirubicin, *J. Fluoresc.*, 2021, **31**(3), 651–658.

40 A. B. Hashkavayi and J. B. Raoof, Design an aptasensor based on structure-switching aptamer on dendritic gold nanostructures/Fe(3)O(4)@SiO(2)/DABCO modified screen printed electrode for highly selective detection of epirubicin, *Biosens. Bioelectron.*, 2017, **91**, 650–657.

41 N. Jandaghi, S. Jahani, M. M. Foroughi, M. Kazemipour and M. Ansari, Cerium-doped flower-shaped ZnO nano-crystallites as a sensing component for simultaneous electrochemical determination of epirubicin and methotrexate, *Mikrochim. Acta*, 2019, **187**(1), 24–34.

42 R. Bavandpour, M. Rajabi and A. Asghari, Electrochemical determination of epirubicin in the presence of topotecan

as essential anti-cancer compounds using paste electrode amplified with Pt/SWCNT nanocomposite and a deep eutectic solvent, *Chemosphere*, 2022, **289**, 133060–133066.

43 S. K. Khalil, Z. Iqbal, N. Niaz and T. Iftikhar, Development and Validation of Reversed-Phase HPLC Method for the Determination of Epirubicin and Its Application to the Pharmacokinetic Study of Epirubicin Loaded Polymeric Nanoparticle Formulations in Rats, *J. Chromatogr. Sci.*, 2023, **61**(3), 249–255.